JOURNAL OF AIRCRAFT
Vol. 35, No. 2, March–April 1998

Formulation of a Comprehensive Aeroelastic Analysis for Tilt-Rotor Aircraft

Venkataraman Srinivas* and Inderjit Chopra†
University of Maryland, College Park, Maryland 20742

A comprehensive aeroelastic analysis is developed to predict the performance, vibratory loads, and aeroelastic stability of composite-coupled advanced-geometry tilt-rotors. Elastic motion of the rotor blades, wing, and fuselage and gimbal motion are modeled. Full wingspan and twin rotors are modeled. Finite element modeling is used along with normal mode reduction to make the analysis robust and efficient. Flight conditions modeled are helicopter (hover and forward flight), conversion, and airplane modes of operation. Predictions from this analysis for trim controls, response, loads, and aeroelastic stability correlate well with flight test data and predictions from other established analyses.

Nomenclature

A = blade cross-sectional area
C = damping matrix
C_T = rotor thrust coefficient
D = drag force
e_d = chordwise offset of aerodynamic center behind elastic axis
F = forcing term
H = rotor drag force
h = pylon height
K = stiffness term, stiffness matrix
L = aerodynamic force, lift force
M = aerodynamic moment, mass matrix
N_b = number of blades
$\hat{\boldsymbol{p}}$ = vector of modal displacements
$\hat{\boldsymbol{q}}$ = vector of discrete displacements
R = blade radius
$\boldsymbol{R}$ = position vector
s = local coordinate
T = kinetic energy
t = time
U = elastic strain energy
u = axial geometric displacement
u_e = axial elastic displacement
$\boldsymbol{V}$ = velocity
v = chordwise (lead-lag) displacement
W = work done, aircraft weight
w = beamwise (flap) displacement
x = longitudinal coordinate
x_h = hub longitudinal motion, positive aft
Y = rotor side force, wing semispan
y_h = hub lateral motion, positive starboard
z_h = hub vertical motion, positive up
α = fuselage angle-of-attack
α_h = hub pitching motion, positive nose-down
α_p = rotor pylon angle, 0 deg for helicopter mode and 90 deg for airplane mode
β = blade flap angle
β_G = gimbal angle in rotating frame
β_{GC} = gimbal angle (cosine) in fixed frame
β_{GS} = gimbal angle (sine) in fixed frame
δ = variation
ε = strain
ζ = blade lag angle
ζ_h = hub yaw motion, positive in direction of rotor rotation in helicopter mode
η, ζ = blade cross-sectional coordinates
θ_{tw} = blade twist
Λ_1 = sweep, positive forward
Λ_2 = anhedral, positive up for dihedral, negative down for anhedral
Λ_3 = pretwist, positive nose-up
μ = advance ratio
σ = stress, rotor solidity, negative decay rate
ϕ = torsional displacement
$\hat{\phi}$ = elastic torsion
ϕ_h = hub roll motion, positive retreating side up in helicopter mode
ψ = blade azimuth angle
Ω = rotor rotational speed, airplane mode
ω = dimensional frequency

Superscripts
$*$ = derivative with respect to azimuth angle
$'$ = derivative with respect to longitudinal coordinate

Presented as Paper 96-1546 at the AIAA/ASME/ASCE/AHS/ASC 37th Structures, Structural Dynamics, and Materials Conference, Salt Lake City, UT, April 15–17, 1996; received Oct. 28, 1996; revision received Sept. 15, 1997; accepted for publication Sept. 19, 1997.

*Research Associate, Alfred Gessow Rotorcraft Center, Department of Aerospace Engineering; currently Senior Project Engineer, Engineering Technology Associates, Madison Heights, MI. Member AIAA.

†Minta–Martin Professor and Director, Alfred Gessow Rotorcraft Center, Department of Aerospace Engineering. Fellow AIAA.

Introduction

TILT-ROTOR aircraft combine the vertical takeoff and landing capability of helicopters with the efficient long-range cruise performance of turboprop fixed-wing airplanes. The tilt-rotor configuration operates in a complex aerodynamic environment over different flight conditions, which results in many performance, aeroelastic, and loads problems. Tilt-rotor aeroelastic instability mechanisms are directly influenced by various rotor and wing design parameters. In addition to conventional aeroelastic instabilities, a unique instability occurs in high-speed axial flight that is referred to as tilt-rotor whirl flutter. This is caused by large unbalanced in-plane rotor forces acting to destabilize the wing.[1–3]

The recent success of the V-22 tilt-rotor program has brought about a surge of interest in other viable tilt-rotor configurations. Advanced tilt-rotors with features such as advanced geometry blades, composite-coupled blades, kinematic blade couplings, and modern rotor hub designs, therefore, need to be investigated to ascertain the possible payoffs. Because of the high expense involved in experimental testing of com-

plex tilt-rotor configurations, it is essential that advanced configurations be investigated using detailed analytical models. Analytical modeling of tilt-rotor aeroelastic behavior is, however, a very challenging task. Many of the earlier analyses[1–3] developed for tilt-rotors were limited in rotor-blade modeling complexity (rigid or elastic), lack of coupled-composite modeling, rotor hub type (articulated, hingeless, or gimballed), flight condition (helicopter or airplane mode), or objective (prediction of performance, loads, detailed aerodynamics, or aeroelastic stability). Other limitations included inability to model complex blade geometry or the complete tilt-rotor system, including the fuselage, full wingspan, and twin-rotor system.[4]

The objective of this paper is to present a comprehensive tilt-rotor aeroelastic analysis that includes 1) modeling of composite couplings, advanced geometry blades, and full configuration (fuselage, wing, and twin-rotor); 2) prediction of performance, vibratory loads, and aeroelastic stability; and 3) coverage of helicopter, conversion, and airplane modes of flight.

Formulation

Elastic blade, wing, and fuselage motion and a twin-rotor model are included in the formulation. The rotor blade is composed of an arbitrary number of Euler–Bernoulli beam segments, each with different sweep, anhedral, pretwist, and planform taper.[5] The formulation handles offsets of blade section c.m., aerodynamic center, and tension center from the elastic axis. Blade kinematic pitch–flap and pitch–lag couplings are also modeled. Highly twisted composite-coupled rotor blades and wings are modeled.

Wing sweep, anhedral, and planform taper are also included in the formulation. Fuselage rigid-body modes as well as elastic modes are included. A full-span wing with twin rotors is modeled to investigate the effects of fuselage motion and wing antisymmetric motion on predicted aeroelastic stability. Because the modeling is performed using finite elements, the analysis is capable of modeling modern rotor hubs, such as bearingless hubs, involving redundant load paths.

Tilt-Rotor Model

An inertial frame of reference is placed on the wing elastic axis (usually at the wingtip) before deformation (Fig. 1). The origin of this frame of reference is at the pivot point of the pylon that is assumed to be on the wing elastic axis. Because the wing itself is flexible, a deformed wing reference frame is required to describe the motion of the wing. This motion is similar to the hub motion in a helicopter.

There are six degrees of freedom at the point at which the rotor pylon connects to the wing, three associated with translations and three with rotations. These six degrees of freedom are similar to hub degrees of freedom of a helicopter, and will henceforth be referred to likewise. The original University of Maryland Advanced Rotorcraft Code (UMARC) formulation[6] has five fuselage degrees of freedom for a helicopter configuration: x_h, y_h, z_h, α_h, and ϕ_h. The new tilt-rotor hub degrees of freedom also include ζ_h.

The hub reference frame is offset from the wing deformed frame by the pylon height and is fixed to the tip of the pylon. The gimballed frame is defined as a transformation oriented at β_{GC} and β_{GS} with respect to the hub fixed-frame. Gimbal motion can be considered as β_G

$$\beta_G = \beta_{GC} \cos\psi + \beta_{GS} \sin\psi \tag{1}$$

For convenience, β_{GC} and β_{GS} are considered part of the hub degrees of freedom, thus making it a total of eight hub degrees of freedom. The gimbal can be locked out of the model when articulated, hingeless, or bearingless rotor configurations are modeled.

There are a total of eight different coordinate systems from the inertial to the deformed blade system.[5] Each coordinate system is related to another through a transformation matrix.

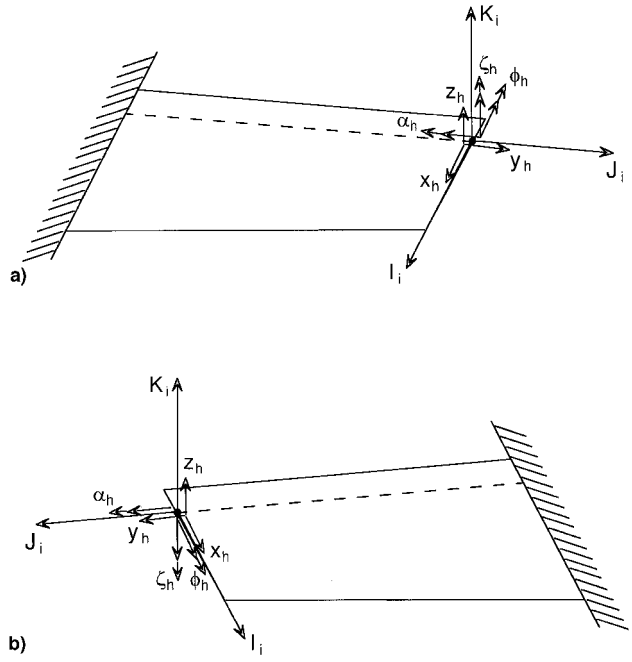

Fig. 1 Right-handed and left-handed reference frames used for a) the right rotor system, and b) the left rotor system.

Advanced Geometry Blades and Wing

Each blade (or wing) segment is assigned a coordinate system to describe its orientation with respect to the main blade control–pitch coordinate system (Fig. 2). The transformation matrix between the undeformed control–pitch frame and the cross-section system with arbitrary Λ_1, followed by Λ_2 and then by Λ_3, is given by

$$[T_\Lambda] = \begin{bmatrix} c_1c_2 & s_1c_2 & s_2 \\ -s_1c_3 - c_1s_2s_3 & c_1c_3 - s_1s_2s_3 & c_2s_3 \\ s_1s_3 - c_1s_2c_3 & -c_1s_3 - s_1s_2c_3 & c_2c_3 \end{bmatrix} \tag{2}$$

where c_i and s_i represent $\cos\Lambda_i$ and $\sin\Lambda_i$, respectively, for $i = 1-3$ for the blade segment.

Coupled-Composite Model

The rotor blades, wing, and fuselage are assumed to be long, slender, anisotropic beams undergoing elastically coupled deformation. The beam may deform elastically in extension u_e, lag bending v, flap bending w, and $\hat{\phi}$, and both built-in pretwist and elastic twist deformation may be large. Elastic stress–strain relationships are given by

$$\begin{Bmatrix} \sigma_{xx} \\ \sigma_{x\zeta} \\ \sigma_{x\eta} \end{Bmatrix} = \begin{bmatrix} Q'_{11} & Q'_{15} & Q'_{16} \\ Q'_{15} & Q'_{55} & Q'_{56} \\ Q'_{16} & Q'_{56} & Q'_{66} \end{bmatrix} \begin{Bmatrix} \varepsilon_{xx} \\ \varepsilon_{x\zeta} \\ \varepsilon_{x\eta} \end{Bmatrix} \tag{3}$$

where Q'_{ij} represent the material stiffnesses at a location on the blade cross section. The matrix $[Q']$ contains all composite-couplings that relate the strains to the stresses. The strain–displacement relations are

$$\begin{aligned} \varepsilon_{xx} &= u'_e + \tfrac{1}{2}(\eta^2 + \zeta^2)\hat{\phi}'^2 + (\hat{\phi}'\lambda_T)' + (\eta^2 + \zeta^2)\theta'_0\hat{\phi}' \\ &\quad - v''[\eta\cos\theta_1 - \zeta\sin\theta_1] - w''[\eta\sin\theta_1 + \zeta\cos\theta_1] \\ \varepsilon_{x\eta} &= v'_s\cos\theta_1 + w'_s\sin\theta_1 + (d\lambda_T/d\eta - \zeta)\hat{\phi}' \\ \varepsilon_{x\zeta} &= w'_s\cos\theta_1 - v'_s\sin\theta_1 + (d\lambda_T/d\zeta + \eta)\hat{\phi}' \end{aligned} \tag{4}$$

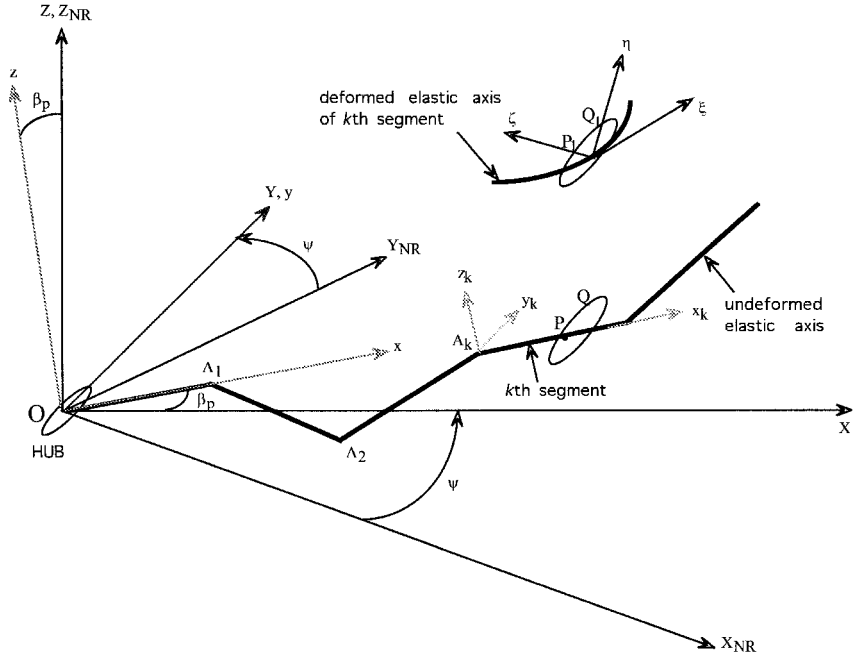

Fig. 2 Coordinate systems for the advanced geometry blade.

where λ_T refers to the torsion-related out-of-plane warping terms, and the subscript s refers to the shear deformation components of the lag and flap degrees of feedom.

Equations of Motion

The tilt-rotor equations of motion were derived from first principles for this study. Derivation of the equations of motion is based on Hamilton's variational principle generalized for a nonconservative system, which can be expressed as

$$\delta\Pi = \int_{t_1}^{t_2} (\delta U - \delta T - \delta W)\, dt = 0 \tag{5}$$

where δW is the work done by nonconservative forces that are of aerodynamic origin. Contributions to these energy expressions from the rotor blades, hub, and wing may be summed as

$$\delta U = \left(\sum_{m=1}^{N_b} \delta U_b\right) + \delta U_h + \delta U_w \tag{6}$$

$$\delta T = \left(\sum_{m=1}^{N_b} \delta T_b\right) + \delta T_h + \delta T_w \tag{7}$$

$$\delta W = \left(\sum_{m=1}^{N_b} \delta W_b\right) + \delta W_h + \delta W_w \tag{8}$$

where the subscripts b, h, and w refer to the blade, hub, and wing, respectively. Fuselage equations of motion are similar to those of the wing.

Strain Energy

Modeling of highly twisted composite-coupled rotor blades is included in the derivation of strain energy. Nonclassical effects such as transverse shear and section warping are captured using a detailed local cross-section analysis, and the effective properties are then used to characterize the global beam analysis.

The variation of the elastic strain energy is given by

$$\delta U = \int_0^R \iint_A \{\sigma_{xx}\delta\varepsilon_{xx} + \sigma_{x\eta}\delta\varepsilon_{x\eta} + \sigma_{x\zeta}\delta\varepsilon_{x\zeta}\}\, d\eta\, d\zeta\, dx \tag{9}$$

Stress–strain relations given by Eq. (3) are substituted into the strain energy variational, which is then expressed in strain terms. The strain–displacement relationship given by Eq. (4) is used to obtain the strain energy variational in terms of the displacement vector. The strain energy expression is then integrated over the cross-sectional area of the blade to obtain linear and nonlinear stiffness terms of the blade equations.

Hub Elastic Strain Energy

The strain energy contribution of the hub is given entirely by the gimbal system when hub springs are included

$$U_h = \tfrac{1}{2} K_{\beta_{GC}} \beta_{GC}^2 + \tfrac{1}{2} K_{\beta_{GS}} \beta_{GS}^2 \tag{10}$$

Other hub degrees of freedom have no strain energy contributions.

Kinetic Energy

Blade velocity components in the three principal directions are derived from first principles. There are two contributions to these velocities: blade motion and hub motion. Hub motion is a resultant of wing and fuselage motion. The expression for the velocity vector of the blade and hub together can be written relative to any frame of reference as

$$\boldsymbol{V} = \boldsymbol{V}_b + \boldsymbol{V}_h \tag{11}$$

where $\boldsymbol{V}_b$ represents the blade contribution and $\boldsymbol{V}_h$ represents the hub contribution to the total velocity.

The position vector of an arbitrary point on the cross section of the deformed blade is written in the inertial reference frame. The contribution of the blade and hub velocities is determined by taking the time derivative of the position vector in the inertial frame. The kinetic energy for the blade and hub system is given by

$$T = \frac{1}{2} \int_0^R \iint_A \rho_s \boldsymbol{V} \cdot \boldsymbol{V}\, d\eta\, d\zeta\, dx \tag{12}$$

where ρ_s is the mass density at any given location in the system. The motion of the wing is coupled to the hub by six wing nodal displacements, which correspond to six hub degrees of

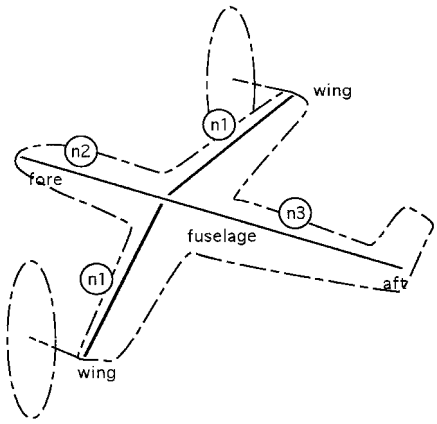

Fig. 3 Schematic of finite element model of fuselage and wing showing number of elements used for each component.

freedom. Details of the derivation of the equations of motion can be found in Ref. 5.

Fuselage Model

The fuselage is modeled as an elastic beam in the longitudinal direction (Fig. 3) using finite elements. Because a finite element model is used, detailed modeling of the empennage can be included at a later stage, if required. Full wingspan is modeled; effects of wing sweep, anhedral, and pretwist are included. Because fuselage motion and full wingspan are modeled, rigid body motion, fuselage elastic motion, and wing symmetric and antisymmetric motion are included in the formulation. Six rigid body degrees of freedom, comprising three translational and three rotational motions, are included. To complete this tilt-rotor model, both left and right systems are modeled (Fig. 3).

A simple drivetrain dynamics model is included. The rotor can be either in the powered condition or in the windmilling condition. Modes of the drive system interconnect shaft are not considered in the analysis. For the windmilling condition, the rotor rotational degree of freedom ϕ_h is independent of wing motion, whereas for the powered case, airplane mode ϕ_h is constrained to the wing bending slope degree of freedom w'.

Twin-Rotor Model

The twin-rotor model for the contrarotating rotors is implemented using the rotor model developed for the right rotor. The tilt-rotor is assumed to be in straight, level flight where the two rotors face exactly the same operating conditions; the trim conditions for the two rotors are, therefore, identical.

Figure 1 shows the coordinate system used for the derivation of the equations of motion for the right rotor system. The rotor/body coupled equations are derived using a right-handed coordinate system. By reversing the direction of the y axis, but maintaining the x and z axes of the right-handed system, the left rotor system could be described in a left-handed system by using the same equations as those used for the right rotor system. As a result of this important simplification, rotor and hub equations for the left rotor can be implemented, as such, in the analysis. Reversal of the y axis for the left rotor, however, changes one hub force direction and two hub moment directions (because ζ_h and ϕ_h are also reversed). Assembly of these equations into the global matrices, therefore, needs to account for changes in these variables. The motion of the left wing semispan is coupled to the left rotor hub by the six wing nodal displacements at the rotor pylon location.

Aerodynamic Model

The aerodynamic formulation is based on quasisteady linear aerodynamic modeling with corrections for unsteady and nonlinear aerodynamics. Local blade velocities are functions of freestream velocity, blade motion relative to the inertial frame, and hub motion relative to the inertial frame. Because blade loads are motion-dependent, they contribute to the system mass, damping, and stiffness matrices as well as to the load vector. Local blade velocities and aerodynamic forces are calculated in the deformed reference frame. This is advantageous because the high-inflow aerodynamics, as seen in the hub frame, can be treated in exactly the same manner in the deformed frame as would the low-inflow aerodynamics in the undeformed frame. Specifically, inflow velocity and the resultant angle of attack in the deformed frame can be assumed to be small, which simplifies the equations to a large extent.

Airfoil section lift, drag, and moment coefficients are obtained from data tables. Mach number effects are included as correction factors to the incompressible section lift, drag, and moment characteristics. Nonlinear compressible aerodynamic effects, such as drag divergence and Mach tuck, can also be included in the form of data tables. Noncirculatory contributions to airloads, arising from pitching and plunging motions of the airfoil section, are also included.

Work performed on the tilt-rotor system is a result of the aerodynamic forces from the rotor system and the wing. Blade airloads associated with blade, gimbal, and hub motion contribute to the mass, damping, and stiffness matrices

$$\delta W_b = \int_0^R (L_u^A \delta u + L_v^A \delta v + L_w^A \delta w + M_\phi^A \delta\hat{\phi})\, \mathrm{d}x \qquad (13)$$

where L_u^A, L_v^A, L_w^A, and M_ϕ^A are the distributed aerodynamic forces acting in the rotating blade reference frame

$$\delta W_h = F_{x_h}\delta x_h + F_{y_h}\delta y_h + F_{z_h}\delta z_h + M_{\alpha_h}\delta\alpha_h + M_{\phi_h}\delta\phi_h + M_{\zeta_h}\delta\zeta_h + M_{\beta_{GC}}\delta\beta_{GC} + M_{\beta_{GS}}\delta\beta_{GS} \qquad (14)$$

where each generalized force is the net load acting on the associated hub degree of freedom. Nonlinear load vectors are linearized about the trim position and contribute to the system stiffness and damping matrices.

Free-Vibration Analysis

A finite element analysis is performed on the system to obtain the natural vibration characteristics. A 15 degree-of-freedom beam element[6] is used to model the blades, wing, and fuselage. Rotor blade natural frequencies and mode shapes are obtained from an eigenanalysis of the structural equations; the normal mode matrix for the blade is denoted by $\mathbf{\Phi}_r$.

The natural vibration analysis of the fuselage/wing is performed independently of the rotor system. The fuselage is considered as a free-free beam spanning from the aft section to the fore section (Fig. 3). The wing is modeled with its root attached to a specified junction of two fuselage elements. The left wing semispan is modeled as a mirror image of the right wing semispan about the fuselage longitudinal axis. The homogeneous system of equations is written as

$$[M_{ff}]^S \ddot{\hat{\boldsymbol{q}}}_f + [K_{ff}]^S \hat{\boldsymbol{q}}_f = 0 \qquad (15)$$

where the superscript S denotes the structural contributions to the matrices. The normal mode matrix for the fuselage/wing is denoted by $\mathbf{\Phi}_f$. Because the free-vibration analysis is performed on a free body (wing attached to a free-free fuselage), the normal mode matrix contains rigid body modes as well as elastic deflection modes.

Coupled-Trim Analysis

The coupled-trim analysis involves simultaneous solution of the vehicle equilibrium equations and the blade steady periodic response equations. The vehicle trim controls depend directly

on the steady aerodynamic loads from the rotor, which are dependent on the blade response. The blade response, in turn, is dependent on the trim control settings. This interdependence between the blade response and trim control angles requires the simultaneous solution of both sets of equations. The vehicle trim equations are nonlinear, and to solve them, initial estimates for the control angles are necessary (because iterative schemes are used). The initial controls estimate is an extremely important step in the trim analysis, as convergence and robustness of the process depend on it. A simple rigid-blade analysis is used to predict the initial trim controls in any steady symmetric flight condition. Based on these initial controls, the elastic blade response equations are solved using a Newton approach along with the vehicle force and moment residual equations.

Trim equations consisting of vehicle force residuals $\hat{F}$ and trim controls $\hat{\theta}$ define the trim state. The force vector defines the equilibrium of the rotor and the airframe forces and moments, which are functions of the trim controls and blade response. There are three types of trim analyses available in this formulation: 1) axisymmetric trim, 2) wind tunnel trim, and 3) free-flight trim. Axisymmetric trim is a very simple scheme applicable to hover (helicopter mode) and airplane modes of operation; the rotor thrust alone is trimmed in this case. Wind tunnel trim assumes a cantilevered wing and a rotor model (excluding the fuselage); the rotor thrust and rotor cyclic flapping are trimmed in this method. The most general trim option is free-flight trim; this method includes a balance of forces and moments from the rotors, wing, fuselage, and empennage.

Figure 4 shows a tilt-rotor in conversion mode of flight and the forces acting on the system. Steady rotor thrust, drag, and pitching moment contribute to the trim equations. Wing, fuselage, and tail incidence angles are included in the trim procedure. Aerodynamic forces from the wing, fuselage, and empennage are thereby included in the equilibrium equations. The horizontal component of the rotor thrust (from both rotors) balances the aircraft drag; the wing lift and vertical component of the rotor thrust balance the weight of the aircraft. The force residual vector for free-flight trim can be written as

Drag:

$$F_1 = (D_f + D_w + D_t)\cos\alpha - (L_f + L_w + L_t)\sin\alpha - (T\sin\alpha_p - H\cos\alpha_p) \tag{16}$$

Thrust:

$$F_2 = (L_f + L_w + L_t)\cos\alpha + (D_f + D_w + D_t)\sin\alpha + (T\cos\alpha_p + H\sin\alpha_p) - W \tag{17}$$

Pitch:

$$F_3 = M_y + M_{yf} - W(z_w\sin\alpha + x_w\cos\alpha) - D_f z_w + M_w + M_t - D_t(z_w - z_t) - L_t(x_t - x_w) + Hh + H[Y_w(\tan\Lambda_{2_w}\cos\alpha_p - \tan\Lambda_{1_w}\sin\alpha_p)] - e_{d_w}(D_w\sin\alpha + L_w\cos\alpha) \tag{18}$$

Roll:

$$F_4 = M_x \tag{19}$$

The lateral force and yaw moment are assumed to be zero, because the aircraft is in symmetric flight about its longitudinal axis. More details on the expressions in these equations can be found in Ref. 5.

Steady rotor response is calculated for a hub-fixed condition. To reduce computational time, blade equations are solved by a normal mode approach using the natural modes calculated in the blade free-vibration analysis. Typically, 5 to 10 normal modes are used. Wing and fuselage steady response is assumed to be zero.

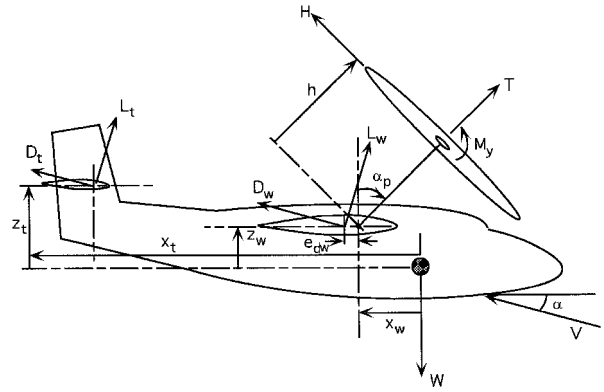

Fig. 4 Forces acting on the tiltrotor in free flight.

The blade response is solved separately in the spanwise and azimuthal directions. Spanwise blade response is obtained as a global vector of discrete displacements (or equivalently in terms of normal modes). Solution for the blade azimuthal response is obtained using a finite element in time procedure. The finite element in time procedure involves transforming differential equations in time into algebraic equations using temporal shape functions.[6]

The rotor wake determines the induced inflow distribution over the rotor disk, and plays a very important role in determining blade response, vibratory loads, acoustic signature, and aircraft performance. Induced inflow depends on the rotor operating condition and is updated in each iteration of the coupled trim analysis. Both momentum theory-based models (such as linear inflow) and vortex models (such as prescribed and free-wake models) have been implemented in the present tiltrotor analysis. The present analysis incorporates a new free-wake analysis developed by Bagai and Leishman.[7] This analysis is based on a pseudoimplicit two-step predictor–corrector scheme that appears to have good numerical convergence characteristics. Details of this free-wake implementation in UMARC are given in Ref. 8.

Rotating blade aerodynamic and inertial loads are calculated and summed using a force summation method in the rotating frame. Blade loads are nonlinear functions of blade displacements, velocities, and accelerations, which are obtained from the solution of the response equations. Loads are then transformed to the fixed frame using a Fourier coordinate transformation. Hub forces are expressed in terms of their harmonics by expanding in terms of Fourier series. Steady components of the hub loads contribute to the vehicle trim equations. Harmonic components of the hub loads are the vibratory loads acting on the airframe.

Stability Analysis

Stability is calculated using a linearized eigenanalysis of the sytem. The linearized perturbed differential equations of motion of the system are derived about the trim condition. Wing sweep, anhedral, and pretwist transformations as well as a twin-rotor model are included.

System equations are written in discrete displacement form as shown next

$$M = \begin{bmatrix} M^{r_1}_{r_1} & M^{i_1}_{r_1} & M^{w_1}_{r_1} & 0 & 0 & 0 & 0 \\ M^{r_1}_{i_1} & M^{i_1}_{i_1} & M^{w_1}_{i_1} & 0 & 0 & 0 & 0 \\ M^{r_1}_{w_1} & M^{i_1}_{w_1} & M^{w_1}_{w_1} & M^{f}_{w_1} & 0 & 0 & 0 \\ 0 & 0 & M^{w_1}_{f} & M^{f}_{f} & M^{w_2}_{f} & 0 & 0 \\ 0 & 0 & 0 & M^{f}_{w_2} & M^{w_2}_{w_2} & M^{i_2}_{w_2} & M^{r_2}_{w_2} \\ 0 & 0 & 0 & 0 & M^{w_2}_{i_2} & M^{i_2}_{i_2} & M^{r_2}_{i_2} \\ 0 & 0 & 0 & 0 & M^{w_2}_{r_2} & M^{i_2}_{r_2} & M^{r_2}_{r_2} \end{bmatrix} \tag{20}$$

$$M \begin{Bmatrix} \ddot{\hat{q}}_{r_1} \\ \ddot{\hat{q}}_{i_1} \\ \ddot{\hat{q}}_{w_1} \\ \ddot{\hat{q}}_f \\ \ddot{\hat{q}}_{w_2} \\ \ddot{\hat{q}}_{i_2} \\ \ddot{\hat{q}}_{r_2} \end{Bmatrix} + C\dot{\hat{Q}} + K\hat{Q} = 0 \tag{21}$$

where the subscripts 1 and 2 refer to the right and left rotor/wing, respectively. The C and K matrices are partitioned in the same manner as the M matrix. Fuselage displacements are contained in $\hat{q}_f$, including the degrees of freedom associated with the wing root attachment to the fuselage

$$\hat{q}_{i_1} = \begin{cases} \begin{Bmatrix} \beta_{GC_1} \\ \beta_{GS_1} \\ \phi_{h_1} \end{Bmatrix} & \text{for windmilling condition} \\ \begin{Bmatrix} \beta_{GC_1} \\ \beta_{GS_1} \end{Bmatrix} & \text{for powered condition} \end{cases} \tag{22}$$

$$\hat{q}_{i_2} = \begin{cases} \begin{Bmatrix} \phi_{h_2} \\ \beta_{GS_2} \\ \beta_{GC_2} \end{Bmatrix} & \text{for windmilling condition} \\ \begin{Bmatrix} \beta_{GS_2} \\ \beta_{GC_2} \end{Bmatrix} & \text{for powered condition} \end{cases} \tag{23}$$

The size of the tilt-rotor problem as solved using a complete finite element method is extremely large, but the computational effort can be significantly reduced by transforming the blade equations into modal space. For this purpose, blade normal modes are recalculated about its mean deflected position, including the effects of nonlinear structural blade couplings. A normal mode reduction is also performed on the fuselage/wing using its normal modes. Rotor displacements can be expressed as

$$\hat{q}_{r_{1_{n\times 1}}} = [\Phi]_{r_{n\times m}} \hat{p}_{r_{1_{m\times 1}}} \tag{24}$$

$$\hat{q}_{r_{2_{n\times 1}}} = [\Phi]_{r_{n\times m}} \hat{p}_{r_{2_{m\times 1}}} \tag{25}$$

where Φ_r is the normal mode matrix for the rotor. Similarly, fuselage/wing displacements can be written as

$$\begin{Bmatrix} \hat{q}_{w_1} \\ \hat{q}_f \\ \hat{q}_{w_2} \end{Bmatrix}_{j\times 1} = [\Phi]_{f_{j\times k}} \hat{p}_{f_{k\times 1}} \tag{26}$$

where $\hat{p}_f$ is the fuselage/wing modal displacement vector and Φ_f is the fuselage/wing normal mode matrix. Rewriting the system of equations in terms of these modal displacement vectors, the equations become

$$\begin{bmatrix} \bar{M}^{r_1}_{r_1} & \bar{M}^{i_1}_{r_1} & \bar{M}^{f}_{r_1} & 0 & 0 \\ \bar{M}^{r_1}_{i_1} & \bar{M}^{i_1}_{i_1} & \bar{M}^{f}_{i_1} & 0 & 0 \\ \bar{M}^{r_1}_{f} & \bar{M}^{i_1}_{f} & \bar{M}^{f}_{f} & \bar{M}^{i_2}_{f} & \bar{M}^{r_2}_{f} \\ 0 & 0 & \bar{M}^{f}_{i_2} & \bar{M}^{i_2}_{i_2} & \bar{M}^{r_2}_{i_2} \\ 0 & 0 & \bar{M}^{f}_{r_2} & \bar{M}^{i_2}_{r_2} & \bar{M}^{r_2}_{r_2} \end{bmatrix} \begin{Bmatrix} \ddot{\hat{p}}_{r_1} \\ \ddot{\hat{q}}_{i_1} \\ \ddot{\hat{p}}_f \\ \ddot{\hat{q}}_{i_2} \\ \ddot{\hat{p}}_{r_2} \end{Bmatrix}$$

$$+ \begin{bmatrix} \bar{C}^{r_1}_{r_1} & \bar{C}^{i_1}_{r_1} & \bar{C}^{f}_{r_1} & 0 & 0 \\ \bar{C}^{r_1}_{i_1} & \bar{C}^{i_1}_{i_1} & \bar{C}^{f}_{i_1} & 0 & 0 \\ \bar{C}^{r_1}_{f} & \bar{C}^{i_1}_{f} & \bar{C}^{f}_{f} & \bar{C}^{i_2}_{f} & \bar{C}^{r_2}_{f} \\ 0 & 0 & \bar{C}^{f}_{i_2} & \bar{C}^{i_2}_{i_2} & \bar{C}^{r_2}_{i_2} \\ 0 & 0 & \bar{C}^{f}_{r_2} & \bar{C}^{i_2}_{r_2} & \bar{C}^{r_2}_{r_2} \end{bmatrix} \begin{Bmatrix} \dot{\hat{p}}_{r_1} \\ \dot{\hat{q}}_{i_1} \\ \dot{\hat{p}}_f \\ \dot{\hat{q}}_{i_2} \\ \dot{\hat{p}}_{r_2} \end{Bmatrix}$$

$$+ \begin{bmatrix} \bar{K}^{r_1}_{r_1} & \bar{K}^{i_1}_{r_1} & \bar{K}^{f}_{r_1} & 0 & 0 \\ \bar{K}^{r_1}_{i_1} & \bar{K}^{i_1}_{i_1} & \bar{K}^{f}_{i_1} & 0 & 0 \\ \bar{K}^{r_1}_{f} & \bar{K}^{i_1}_{f} & \bar{K}^{f}_{f} & \bar{K}^{i_2}_{f} & \bar{K}^{r_2}_{f} \\ 0 & 0 & \bar{K}^{f}_{i_2} & \bar{K}^{i_2}_{i_2} & \bar{K}^{r_2}_{i_2} \\ 0 & 0 & \bar{K}^{f}_{r_2} & \bar{K}^{i_2}_{r_2} & \bar{K}^{r_2}_{r_2} \end{bmatrix} \begin{Bmatrix} \hat{p}_{r_1} \\ \hat{q}_{i_1} \\ \hat{p}_f \\ \hat{q}_{i_2} \\ \hat{p}_{r_2} \end{Bmatrix} = 0 \tag{27}$$

where

$$\begin{aligned} \bar{M}^{r_1}_{r_1} &= [\Phi]^T_r M^{r_1}_{r_1} [\Phi]_r \\ \bar{M}^{i_1}_{r_1} &= [\Phi]^T_r M^{i_1}_{r_1} \\ \bar{M}^{f}_{r_1} &= [\Phi]^T_r [M^{w_1}_{r_1}\ M^{f}_{r_1}\ M^{w_2}_{r_1}] [\Phi]_f \\ \bar{M}^{r_1}_{i_1} &= M^{r_1}_{i_1} [\Phi]_r \\ \bar{M}^{f}_{i_1} &= [M^{w_1}_{i_1}\ M^{f}_{i_1}\ M^{w_2}_{i_1}] [\Phi]_f \\ \bar{M}^{r_1}_{f} &= [\Phi]^T_f \begin{Bmatrix} M^{r_1}_{w_1} \\ M^{r_1}_{f} \\ M^{r_1}_{w_2} \end{Bmatrix} [\Phi]_r \\ \bar{M}^{i_1}_{f} &= [\Phi]^T_f \begin{Bmatrix} M^{i_1}_{w_1} \\ M^{i_1}_{f} \\ M^{i_1}_{w_2} \end{Bmatrix} \\ \bar{M}^{f}_{f} &= [\Phi]^T_f \begin{bmatrix} M^{w_1}_{w_1} & M^{f}_{w_1} & M^{w_2}_{w_1} \\ M^{w_1}_{f} & M^{f}_{f} & M^{w_2}_{f} \\ M^{w_1}_{w_2} & M^{f}_{w_2} & M^{w_2}_{w_2} \end{bmatrix} [\Phi]_f \end{aligned} \tag{28}$$

$$\hat{Q}' = \begin{Bmatrix} \hat{p}_{r_1} \\ \hat{q}_{i_1} \\ \hat{p}_f \\ \hat{q}_{i_2} \\ \hat{p}_{r_2} \end{Bmatrix} \tag{29}$$

The system mass, damping, and stiffness matrices given in (27) are referred to as M', C', and K', respectively. Matrices C' and K' are expressed, similar to M', in terms of the partitioned C and K matrices, respectively.

Floquet theory and constant coefficient solution methods are implemented in the analysis. Constant coefficient assumption is valid in investigating whirl flutter instability, because whirl flutter occurs in high-speed forward flight when the flow about the rotor is almost axisymmetric, and the system equations are independent of the rotor blade azimuth angle. Floquet theory, however, can be used when necessary.

Results

The analysis described in this paper was used to obtain results for the XV-15 tilt-rotor configuration in the airplane mode of operation. Important rotor and wing parameters for the XV-15 are given as follows: 1) rotor properties—rotor type, gimballed; number of blades, 3; radius (R), 12.5 ft; lock number, 3.83; solidity, 0.089; pitch-flap coupling, -0.268 ($\delta_3 = -15$ deg); hub precone, 2.5 deg; root cutout, 10%; rotor speed, 517 rpm; and 2) wing properties—semispan/R, 1.333; chord/R, 0.413; pylon height/R, 0.342. The first free-vibration blade mode (predominantly lag) frequency predicted by the present analysis is 1.432 per rev, compared with 1.329 per rev calculated in Ref. 9. Flap, lag, and torsional components are fully coupled in the blade mode shapes because of the large blade pretwist, as well as the high rotor collective pitch and c.g. offsets from the elastic axis.

Trim Controls and Rotor Loads

Results presented in this section were obtained using the present analysis with the free-flight trim option. Because the aircraft is in free flight at different airspeeds, the pitch attitude as well as the rotor collective and cyclic pitch inputs are adjusted to achieve aircraft equilibrium. This was done during

the XV-15 flight test.[10] The XV-15 configuration was also flight tested with rigged (fixed) cyclic pitch controls, results for which are not presented in this paper. In that case, only rotor collective pitch and aircraft pitch attitude are trim variables in a symmetric free-flight condition (similar to that in a turboprop airplane).

Figure 5 shows the predicted variation of aircraft pitch attitude with airspeed in airplane mode. Flight test data and predictions from Bell Helicopter Co.'s C81 analysis[10] are also shown in the figure. The flight test included the use of wing flaps below an airspeed of 190 kn. The C81 analysis included detailed aerodynamic modeling of the rotor/wing/fuselage interference effects as well as wing flaps, which the present analysis has neglected. Despite the usage of simplified aerodynamics, good correlation is obtained from the present analysis for the variation of pitch attitude with airspeed. It should be pointed out that the flight test data show considerable scatter and are available only over a limited range of airspeed.

Variation of rotor collective pitch and longitudinal gimbal flapping with airspeed is shown in Figs. 6 and 7, respectively. Figure 6 shows that the rotor collective, required to trim the aircraft in steady level flight, increases considerably with increasing airspeed. At higher airspeeds, the forward speed contribution to rotor total inflow increases. Higher rotor collective pitch is, therefore, required to trim the aircraft to the required thrust. The figure shows that predictions from the present analysis correlate well with flight test data and C81 predictions. Figure 7 shows that the present analysis predicts the variation of longitudinal gimbal flapping very well.

Figure 8 shows the variation of predicted rotor torque (per rotor) with airspeed. Predictions from the present analysis with and without a 3% tip loss factor are shown in the figure. Overall, the predictions correlate very well with flight test data and with C81 predictions. More validation studies for trim controls and rotor loads are available in Ref. 5.

Aeroelastic Stability

The aeroelastic stability in high-speed airplane mode was investigated for the occurrence of whirl flutter. Wing symmetric motion occurs when the left wingtip deformation is in the same direction as the right wingtip deformation. Wing antisymmetric motion, on the other hand, occurs when the left wingtip deformation is in the opposite direction as the right wingtip deformation. Tilt-rotor high-speed instabilities are caused by rotor forces destabilizing the wing modes and consequent wing motion feeding back to affect rotor stability.

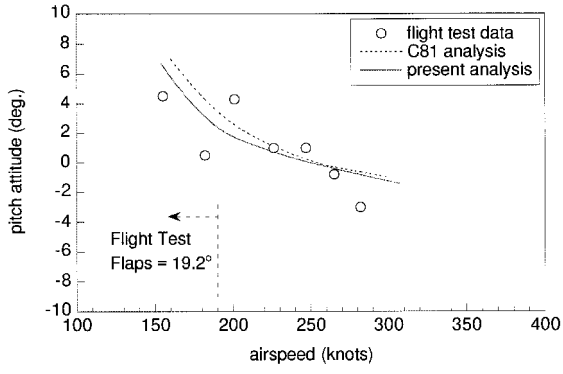

Fig. 5 Aircraft pitch attitude variation with airspeed.

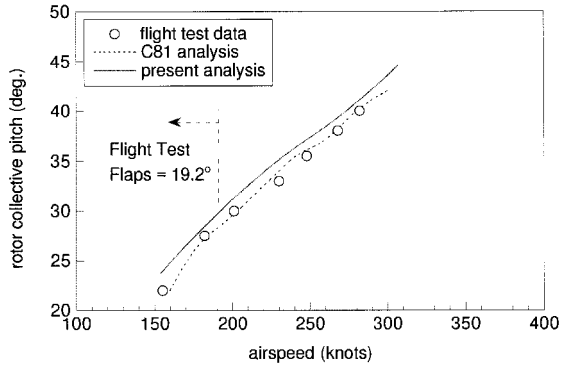

Fig. 6 Rotor collective variation with airspeed.

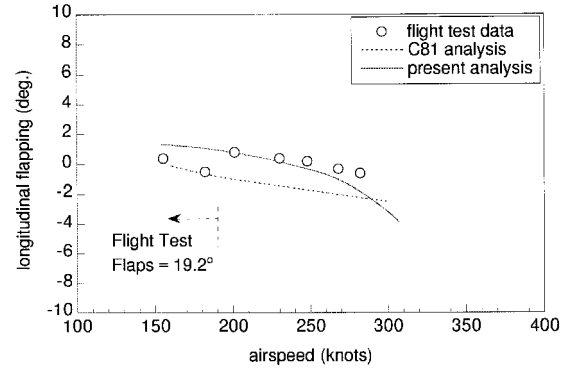

Fig. 7 Rotor longitudinal flapping variation with airspeed.

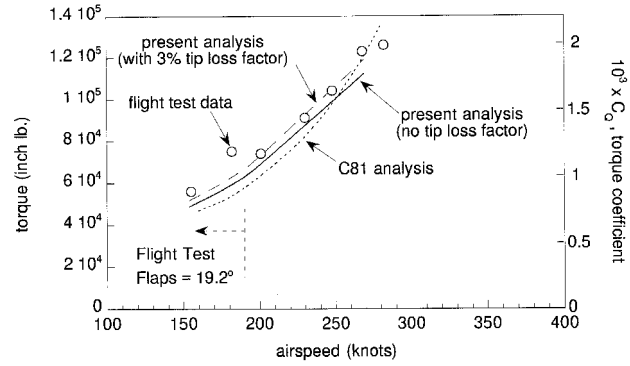

Fig. 8 Rotor torque variation with airspeed.

Some validation studies were performed with available test data and predictions from other established analyses. Figures 9 and 10 show the predicted stability frequencies and damping ratios of the wing symmetric and antisymmetric beam bending modes. Predictions from DYN4, DYN5, and proprotor aeroelastic stability analysis (PASTA), as well as XV-15 flight test data from Ref. 10, are shown in the figures. Both DYN4 and PASTA are rigid-blade tilt-rotor analyses, whereas DYN5 analysis includes rigid-blade modes as well as elastic modes. The data were taken at an altitude of 10,000 ft for a windmilling rotor condition. Windmilling flight condition is modeled by the analyses assuming the collective lag angle to be a degree of freedom. DYN4 and PASTA model only windmilling flight conditions, whereas DYN5 and the present analysis can model both windmilling and powered flight. Five finite elements were used to model each wing semispan and two elements were used to model the fuselage in the present analysis. Each rotor blade was modeled using six finite elements. Fifteen coupled fuselage/wing modes, including the six coupled rigid-body modes and nine coupled elastic modes, were used in the stability predictions in the present analysis. The fuselage/wing elastic modes used in the analysis included the fundamental symmetric and antisymmetric modes of wing beam, chord, and torsion motion.

Figure 9 shows that all the analyses predict the wing symmetric beam frequencies well. Figure 10 shows the variation of damping ratio with forward flight speed for the wing symmetric beam mode. The DYN4 analysis overpredicts the damping considerably, whereas predictions from the other analyses correlate well with the limited test data. The reason for this overprediction could not be ascertained from available literature on these analyses. It should be pointed out that the flight

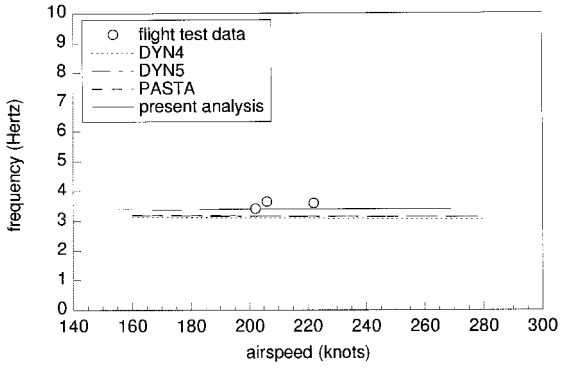

Fig. 9 Variation of wing symmetric beam mode frquencies with airspeed.

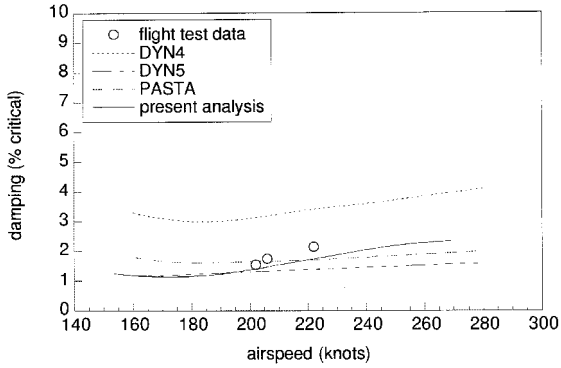

Fig. 10 Variation of wing symmetric beam mode damping with airspeed.

test data show considerable scatter and are available over only a limited range of airspeed.

Summary and Conclusions

The elastic tilt-rotor model developed in this study handles highly twisted composite-coupled advanced-geometry blades for tilt-rotors in helicopter mode (including hover), airplane mode, and conversion mode. An analysis capable of modeling the dynamics of such tilt-rotors and predicting the system response, loads, and aeroelastic stability has been formulated. The advanced-geometry rotor model can be used for blades with arbitrary variation of sweep, anhedral, pretwist, and planform taper with span; blade modeling is performed using finite elements. The formulation handles offsets of blade section c.m., aerodynamic center, and tension center from the elastic axis. The tilt-rotor wing can also have sweep, anhedral, pretwist, and planform taper, and is modeled using finite elements. The rotor hub is capable of motion along six degrees of freedom. The formulation has the capability to model gimballed tilt-rotors as well as rotors with articulated, hingeless, and bearingless hubs. An elastic fuselage is modeled using beam finite elements. Airframe rigid body modes as well as fuselage and wing elastic motions are included. Wing symmetric and antisymmetric modes are considered in the solution procedure. A twin-rotor model is included. Momentum-based rotor inflow models as well as vortex-based inflow models (such as prescribed and free-wake models) are implemented in the analysis. Trim schemes included are axisymmetric trim, wind-tunnel trim, and free-flight trim.

Some sample validation results have been presented in the paper. The following conclusions are drawn from these results:

1) Aircraft pitch attitude and rotor collective predicted by the present analysis correlate satisfactorily with C81 predictions and with flight test data.

2) Rotor longitudinal flapping and rotor torque predicted by the present analysis correlate well with flight test data.

3) Variation of wing beam mode frequencies is predicted well by all the analyses considered in the study. The damping is underpredicted.

More validation studies, parametric studies, and detailed conclusions that encompass the full scope of the present analysis are available in Ref. 5.

Acknowledgments

The authors acknowledge the support for this research work by the U.S. Army Research Office under Center for Rotorcraft Education and Research Contract DAAH-04-94-G-0074; Technical Monitor was Tom Doligalski. The authors also thank Jing Yen and John Corrigan of Bell Helicopter Co. for providing data, and Mark Nixon of the NASA Langley Research Center for valuable technical discussions.

References

[1]Gaffey, T. M., Yen, J. G., and Kvaternik, R. G., "Analysis and Model Tests of the Proprotor Dynamics of a Tilt-Proprotor VTOL Aircraft," U.S. Air Force V/STOL Technology and Planning Conf., Las Vegas, NV, Sept. 1969.

[2]Kvaternik, R. G., "Studies in Tilt-Rotor VTOL Aircraft Aeroelasticity," Ph.D. Dissertation, Case Western Reserve Univ., Cleveland, OH, 1973.

[3]Johnson, W., "Dynamics of Tilting Proprotor Aircraft in Cruise Flight," NASA TN D-7677, May 1974.

[4]Nixon, M. W., "Aeroelastic Response and Stability of Tiltrotors with Elastically Coupled Composite Rotor Blades," Ph.D. Dissertation, Dept. of Aerospace Engineering, Univ. of Maryland, College Park, MD, Dec. 1993.

[5]Srinivas, V., "Aeroelastic Analysis of Advanced Tiltrotor Aircraft," Ph.D. Dissertation, Dept. of Aerospace Engineering, Univ. of Maryland, College Park, MD, 1995.

[6]Bir, G. S., and Chopra, I., "University of Maryland Advanced Rotorcraft Code (UMARC)," *Theory Manual*, Center for Rotorcraft Education and Research, Univ. of Maryland, College Park, MD, 1994.

[7]Bagai, A., and Leishman, J. G., "Rotor Free-Wake Modeling Using a Pseudo-Implicit Relaxation Algorithm," AIAA Paper 94-1918, June 1994.

[8]Srinivas, V., "The UM Free-Wake Analysis in UMARC," Dept. of Aerospace Engineering, Univ. of Maryland, UM-AERO Rept. 95-26, College Park, MD, July 1995.

[9]Johnson, W., "Analytical Modeling Requirements for Tilting Proprotor Aircraft Dynamics," NASA TN D-8013, 1975.

[10]"XV-15 Full Scale Test Data Correlation Report," Bell–Boeing, Joint Project Office Rept. 901-909-003, Ft. Worth, TX, Nov. 1985.